CARBON 49 (2011) 587–598

available at www.sciencedirect.com

ScienceDirect

journal homepage: www.elsevier.com/locate/carbon

Synthesis and characterization of iron-impregnated porous carbon spheres prepared by ultrasonic spray pyrolysis

John D. Atkinson [a], Maria E. Fortunato [b], Seyed A. Dastgheib [c,*], Massoud Rostam-Abadi [a,c], Mark J. Rood [a], Kenneth S. Suslick [b,*]

[a] Department of Civil and Environmental Engineering, University of Illinois, 205 N. Mathews Ave., Urbana, IL 61801, USA
[b] Department of Chemistry, School of Chemical Sciences, University of Illinois, 600 S. Mathews Ave., Urbana, IL 61801, USA
[c] Advanced Energy Technology Initiative, Illinois State Geological Survey, Institute of Natural Resource Sustainability, University of Illinois, 615 E. Peabody Dr., Champaign, IL 61820, USA

ARTICLE INFO

Article history:
Received 5 August 2010
Accepted 1 October 2010
Available online 8 October 2010

ABSTRACT

Porous carbon microspheres impregnated with iron-based nanoparticles are prepared in a single step, continuous process using ultrasonic spray pyrolysis (USP). Precursor solutions containing a carbon source, an inorganic salt, and an iron salt are ultrasonically aerosolized and pyrolyzed. Solutions containing nitrate or chloride salts are examined. During pyrolysis, sucrose is dehydrated to carbon, and the metal salt is converted to crystalline or non-crystalline iron species, depending on processing conditions. The product's porosity is generated from: (1) aromatization of carbon around an *in situ* template, (2) *in situ* gasification of isolated carbon, or (3) *in situ* chemical activation of the carbon precursor. Porous carbon spheres (0.5–3 μm diameter) containing well-dispersed iron oxide nanoparticles (4–90 nm diameter), referred to here as Fe–C, are prepared. Iron loadings between 1 and 35 wt.% are achieved while maintaining well-dispersed Fe nanoparticles with as-produced surface areas up to 800 m^2/g. Post-pyrolysis heat and hydrogen treatments increase the surface area of the materials while reducing iron species. USP Fe–C materials may have useful catalytic applications due to their potential for high-loading of well-dispersed metal nanoparticles. Despite negligible surface Fe content, chromium reduction tests indicate that internal Fe sites are catalytically active.

© 2010 Elsevier Ltd. All rights reserved.

1. Introduction

Nanosized particles exhibit different, often enhanced, magnetic, electronic, optical, and reactive properties compared to corresponding bulk materials, making them desirable for applications including catalysis, adsorption, ferrofluids, electronic sensing, medical applications, and drug delivery [1–7]. For many applications, transition metals provide a distinct advantage over precious metals because of their decreased costs. Interest in iron nanoparticles originates from iron's magnetic properties, its ready availability and low cost, and its high reactivity, particularly in reducing atmospheres [1,7,8]. Specific applications for iron nanoparticles include Fischer–Tropsch catalysts, oxygen reduction catalysts in fuel cells, environmental adsorbents for CO or arsenic, and catalysts for CO oxidation or destruction of polychlorinated dibenzodioxins or dibenzofurans (PCDDs/PCDFs) [2,7,9–13].

Dispersing iron nanoparticles onto a support can enhance the iron's available surface area, resulting from an increase in the metal's surface to volume ratio. Porous carbon can be an especially effective support because it provides high surface area, it is resistant to both acidic and basic conditions, its surface can be functionalized to provide controlled metal loading sites, its pore structure can be tailored for enhanced

* *Corresponding authors:* Fax: +1 217 333 8566 (S.A. Dastgheib), +1 217 244 3186 (K.S. Suslick).
E-mail addresses: seyed@isgs.illinois.edu (S.A. Dastgheib), ksuslick@illinois.edu (K.S. Suslick).
0008-6223/$ - see front matter © 2010 Elsevier Ltd. All rights reserved.
doi:10.1016/j.carbon.2010.10.001

adsorption, it is stable at high temperatures in anoxic conditions, and it can be combusted to recover spent catalysts [14]. Disadvantages of carbon supports include combustion in the presence of oxygen and a potential loss of selectivity from metal impurities in ash [14,15]. Metal-impregnated carbon materials are typically prepared in a multi-step process: (1) carbonization of an organic precursor, (2) physical or chemical activation of the carbon product, (3) catalyst impregnation (using excess solution, incipient wetness, ion exchange, or chemical vapor deposition techniques), and (4) reduction or pyrolysis to form metal nanoparticles [16]. The process is usually non-continuous and can require substantial time and energy. Each step requires heat, and the carbon activation stage requires supplemental reagents to develop porosity. It is advantageous to simplify this process to allow continuous production of metal-impregnated, porous carbon materials.

Aerosol techniques can provide simple, scalable, and continuous methods for porous carbon production [17–23]. Ultrasonic spray pyrolysis (USP) has been used to directly prepare porous carbon spheres (0.5–3 μm diameter) from a variety of organic salt precursors [24–26]. Meso- and macroporosity are developed using *in situ* templates and microporosity results from *in situ* carbon gasification. Bang et al. impregnated USP carbon with PtRu catalysts by incipient wetness to improve the activity of a direct methanol fuel cell anode [27]. In contrast, Liu and coworkers used USP to impregnate a commercial activated carbon with a catalyst precursor while activating the catalyst [28]. Others have reported using USP as an impregnation technique for fuel cell catalysts [29].

Progressing towards the goal of a one-step, metal-impregnated porous carbon preparation, Yu et al. recently prepared Fe_xO_y@C spheres using a low temperature process where sucrose is catalytically dehydrated while iron oxide nanoparticles are dispersed within the carbon spheres [30]. This process, however, did not provide high internal porosity within the carbon spheres and resulted in a low surface area material (42 m^2/g). Post-production hydrogen treatment was used to partially gasify the carbon to add surface area (189 m^2/g) and reduce iron oxides. Their process, unfortunately, does not allow for simultaneous porosity development during the sucrose carbonization and catalyst impregnation steps. There are also several continuous techniques (many that utilize spray pyrolysis) for preparing *carbon-encapsulated* magnetic nanoparticles (CEMNs), but high surface areas and high iron loadings are not reported for materials prepared by these methods [31–35].

We report here a novel USP synthesis that allows for continuous production of high surface area, porous carbon spheres impregnated with well-dispersed iron nanoparticles (abbreviated as Fe–C). This technique provides an alternative method for producing iron-impregnated carbon materials in a simple and continuous process. An organic precursor is carbonized, porosity is formed *in situ*, iron is dispersed within the carbon spheres, and metal nanoparticles are activated – all in a continuous flow synthesis with aerosol residence times on the order of seconds. The main objectives of this paper are to describe the Fe–C preparation method, characterize the physical and chemical properties of the iron-loaded carbon products, and describe potential applications for the materials.

2. Methodology

2.1. Precursor preparation

Sucrose (Sigma–Aldrich, 99.5%; EMD Chemicals, ACS grade), sodium chloride (Sigma–Aldrich, 99%), anhydrous iron (III) chloride (Fisher, 97%), sodium nitrate (Fisher, Certified ACS), and iron (III) nitrate nonahydrate (Sigma–Aldrich, 98+%) were used as purchased. Two precursor solutions were prepared by dissolving sucrose, the inorganic salt (NaCl or $NaNO_3$), and the iron salt ($FeCl_3$ or $Fe(NO_3)_3$) in deionized water. Unless otherwise noted, the chloride-based precursor solution contained 0.6 M sucrose and 2.4 M NaCl, and the nitrate-based precursor contained 0.5 M sucrose and 1.0 M $NaNO_3$. $FeCl_3$ concentrations in the chloride precursor solutions were varied from 0 to 0.39 M and $Fe(NO_3)_3$ concentrations in the nitrate precursor solutions were varied from 0 to 0.12 M. Precursor solutions containing iron species were acidic ($1 < pH < 3$).

Precursor solutions containing transition metals other than iron were prepared using sucrose and $Co(NO_3)_2{\cdot}6H_2O/NaNO_3$, $Ni(NO_3)_2{\cdot}6H_2O/NaNO_3$, $Cu(CH_3OO)_2$/NaCl, or $Zn(CH_3OO)_2$/NaCl. All metal salts were ⩾99% pure. Sucrose and NaCl or sucrose and $NaNO_3$ concentrations were consistent with the iron precursor solutions.

2.2. USP apparatus

The USP system is similar to one described elsewhere [24]. The precursor solution was ultrasonically nebulized and the resulting aerosol was entrained in an inert gas stream (Ar or N_2) and carried into a preheated (500–900 °C) quartz tube reactor (L = 33 cm, ID = 30 mm) inserted inside an insulated tube furnace. A horizontal furnace was used with chloride-based precursors and a vertical furnace was used with nitrate-based precursors. Gas flow rate was controlled by a rotameter and was 1.67×10^{-5} m^3/s (1 SLPM) unless otherwise noted; aerosol residence times in the tube reactor heating zone were <7 s. Pyrolysis products were collected in deionized water bubblers. The carbon-based products from chloride precursors were isolated by vacuum filtration and dried overnight in air at 110 °C and ambient pressure before analysis. The products from nitrate precursors were isolated by centrifugation (Fisher Model 225, <5000 rpm), washed with at least four aliquots of deionized water/ethanol, and dried under vacuum at 60 °C overnight before analysis.

2.3. Fe–C heat and hydrogen treatments

Fe–C was placed in a glass cell and purged with nitrogen at room temperature for >1 h before heating at 400 °C under nitrogen or hydrogen for 12–16 h. After heating, the cell was allowed to cool to room temperature under a nitrogen flow and the Fe–C was removed from the cell for analysis.

2.4. Fe–C iron leaching experiments

Fe–C prepared from chloride and nitrate-based precursors at 700 °C were tested for stability in acidic solutions. Twenty-five milligrams of Fe–C was dispersed in 10 mL of 0.1 M NaCl solution and HCl was added to adjust the solution to pH 2. The

vials were continuously agitated on a Barnstead/Thermadyne Labquake® Rotisserie. After 48 h, the dispersions were filtered using a 0.02 μm filter. The acidic leaching solutions were analyzed by inductively couple plasma optical emission spectroscopy (ICP-OES).

2.5. Material characterization

Surface morphology of the Fe–C products was observed using scanning electron microscopy (SEM, JEOL 7000F) at 15 kV. SEM samples were prepared by dispersing Fe–C in ethanol, placing the dispersion on a silicon wafer, and evaporating the ethanol. Samples were coated with 10 nm of AuPd prior to analysis to prevent surface charging. Iron nanoparticle diameter was qualitatively determined using transmission electron microscopy (TEM, JEOL 2100) at 200 kV. TEM samples were prepared by dispersing Fe–C in ethanol, dipping a lacy formvar/carbon–copper grid into the dispersion, and drying the grid overnight before analysis.

Crystalline iron species were identified with powder X-ray diffraction (XRD, Siemens-Bruker D5000) using Cu Kα radiation (λ = 1.5415 Å) with a step size of 0.05° and a scan rate of 0.4°/min. The diffraction peaks were indexed using the ICDD database. When appropriate, MDI Jade 9 software was used to calculate the crystallite size of the iron species using the Scherrer equation and the relative amounts of the iron species were determined by integrating under the diffraction peaks.

N_2 adsorption isotherms were measured at 77 K using a surface area analyzer (Quantachrome Nova 2200e). Carbon samples were degassed under vacuum for 16–24 h at 110 °C before analysis. BET surface area was calculated from adsorption data in relative pressures range of $0.05 < P/P_0 < 0.2$. A single point ($P/P_0 = 0.3$) BET analyzer (Quantachrome, Monosorb) was also used to obtain N_2 BET surface areas.

Bulk elemental analysis was performed by the University of Illinois' School of Chemical Sciences Microanalysis Laboratory. CHN analysis was performed using a Model CE-440 CHN analyzer (Exeter Analytical, Inc.). Bulk iron content of microwave digested Fe–C samples was determined using inductively coupled plasma mass spectroscopy (ICP-MS, Perkin–Elmer – Sciex Elan DRCe).

The surface composition of select Fe–C materials was analyzed with X-ray photoelectron spectroscopy (XPS, Kratos Axis Ultra).

2.6. Cr(VI) solution preparation and reduction experiments

Select Fe–C samples were treated with a Cr(VI) solution to examine their potential for use in liquid-phase reduction applications. $K_2Cr_2O_7$ (ACS grade) was dried at 180 °C under vacuum for 2 h. A 34 μM Cr(VI) solution was prepared by dissolving dried $K_2Cr_2O_7$ in deionized water. Dispersions of reduced Fe–C in 34 μM Cr(VI) solution (10:3 Fe:Cr molar ratio) were prepared in a glove box. As a control, reduced USP carbon (no iron present, used same carbon mass as in Fe–C dispersions) was also dispersed in a 34 μM Cr(VI) solution. The vials were continuously agitated on a Barnstead/Thermadyne Labquake® Rotisserie. At timed intervals, dispersions were removed for analysis.

Cr(VI) concentrations were determined using UV–vis spectrometry (Varian Cary 50) following EPA method 7196a [36]. Cr(VI) sample solutions were extracted from the bulk dispersions and filtered with a 0.22 μm filter. A 10 mL volume of the extracted Cr(VI) solution was mixed with 2 mL of a 0.02 M solution of 1,5-diphenylcarbazide in acetone and the pH was adjusted to 1–2 by addition of a 10% v/v sulfuric acid solution. Cr(VI) calibration solutions were filtered and prepared using the same method.

3. Results and discussion

3.1. Materials characterization

Iron-impregnated porous carbon microspheres (Fe–C) prepared using USP are <3.0 μm in diameter (Fig. 1), and their physical properties are summarized in Table 1. TEM (Fig. 2) shows that iron nanoparticles are dispersed within the porous carbon support; diameters of the iron nanoparticles vary with the precursor composition and reactor temperature, and are observed by TEM to range from <20 to 90 nm (Figs. 2 and 3). XPS indicates that no iron is present on the carbon surface. A negligible amount of sodium in XPS data confirms that the washing procedure removes all surface salts.

Major differences in the surface morphology of Fe–C products synthesized from the two precursor solutions are evident by SEM. For materials prepared using chloride salts, external surface heterogeneities are generated because solid sodium chloride acts as an *in situ* template during Fe–C production (Fig. 1a–d). As water evaporates from the aerosol droplets, NaCl, which is present at a high concentration, precipitates out at the surface, allowing for generation of visible surface heterogeneities. Washing removes the template, leaving external carbon porosity, which is visible on the surface of Fe–C prepared from chloride-based precursors at all temperatures. In the absence of such a salt template (i.e., no NaCl added), the Fe–C samples prepared have a smooth exterior surface morphology (Fig. 4a).

In contrast to Fe–C prepared from chloride-based precursor solutions, materials prepared using nitrate salts do not show such highly textured surface morphologies (Fig. 1e–h). Compared to NaCl in the chloride precursors (2.4 M), $NaNO_3$ is present in lower concentrations (1 M). $NaNO_3$ is also more soluble than NaCl, which prevents its rapid precipitation to the surface of the drying aerosol particles. This limits the development of surface heterogeneities. Molten NaOH is expected to form as a by-product of $NaNO_3$ decomposition at >600 °C, but its presence does not appear to impact the Fe–C surface morphology. Fe–C materials prepared with or without $NaNO_3$ have a similar surface morphology (Figs. 1g and 4b).

XRD patterns of Fe–C products prepared from chloride or nitrate salts at 500–800 °C (corresponding to Table 1) are shown in Fig. 5. A broad peak at 2θ angles between 10° and 30° is not shown in Fig. 5, but is consistent for all Fe–C materials and corresponds to amorphous carbon. No graphitic carbon was formed (i.e., no corresponding sharp diffraction peak at 26–27° was observed in any Fe–C XRD pattern), most likely

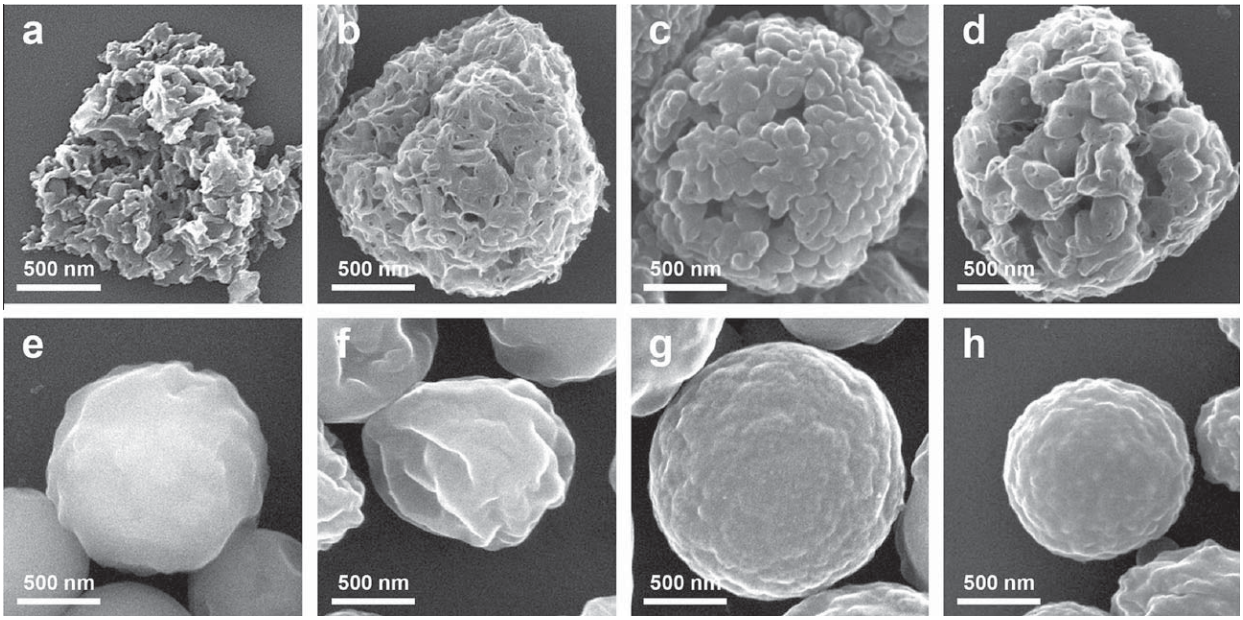

Fig. 1 – SEM images of Fe–C described in Table 1 and prepared by USP using (a–d) chloride-based precursors and (e–h) nitrate-based precursors at 500, 600, 700, and 800 °C (left to right).

Table 1 – Production parameters, surface area, and impregnated iron characteristics of Fe–C materials prepared using chloride or nitrate-based precursors at select temperatures and a carrier gas flow rate of 1 SLPM.

Figs. 1 and 2 label	Anion	Temp. (°C)	Precursor iron conc. (M)	Production rate (mg/50 mL)[a]	BET S.A.[b] (m^2/g)	Iron form	Iron nanoparticle diameter (nm)
a	Chloride	500	0.12	275	140	Amorphous	–
b	Chloride	600	0.12	240	320	Fe_3O_4	<20
c	Chloride	700	0.12	210	560	Fe_3O_4	<20
d	Chloride	800	0.12	110	800	Fe_3O_4	<20
e	Nitrate	500	0.02	800	4	Amorphous	–
f	Nitrate	600	0.02	530	40	Fe_3O_4 $Fe_{1-x}O$	<20
g	Nitrate	700	0.02	330	680	Fe_3O_4 $Fe_{1-x}O$ Fe_2N	<20
h	Nitrate	800	0.02	70	740	Fe_3O_4 $Fe_{1-x}O$ Fe_2N	30–90

[a] mg Fe–C product collected per 50 mL precursor solution aerosolized.
[b] S.A. = surface area.

due to short residence times and moderate temperatures preventing carbon crystallization.

Fe–C prepared using chloride salts at the lowest temperature (500 °C) does not show a crystalline iron phase, but the presence of iron is confirmed by bulk elemental analysis (Fig. 5a, Table 2). At higher temperatures (600–800 °C), the presence of identifiable, iron-associated XRD peaks for materials prepared using the chloride salts indicates that crystalline iron is present; these peak locations match the standard for magnetite (Fe_3O_4, PDF#04-005-4319). Peaks corresponding to NaCl (halite) were not observed. Crystalline zero valent iron, iron carbide, hematite, or wustite were not observed for Fe–C materials prepared from chloride-based salts.

Fe–C prepared using nitrate salts at 500 °C also does not show a crystalline iron phase, but the presence of iron is again confirmed by bulk elemental analysis (Fig. 5b, Table 2). The presence of identifiable, iron-associated peaks in the patterns for materials prepared using nitrate salts at 600–800 °C indicates that crystalline iron is present; these peak locations match the standards for Fe_3O_4 and a reduced wustite phase ($Fe_{1-x}O$, e.g., PDF#01-085-0625). Additionally, peaks matching iron nitride (ζ-Fe_2N, PDF#04-011-7278) are found in the patterns for the Fe–C materials prepared at 700 and 800 °C. The relative intensity of the $Fe_{1-x}O$ peaks decreases and the relative intensity of the Fe_2N peaks increases as the pyrolysis temperature increases, but Fe_3O_4 is the dominant crystalline iron species regardless of preparation temperature. Peaks representing residual or trapped $NaNO_3$ or NaOH (formed during sodium nitrate decomposition) are not seen, indicating complete decomposition or removal after the washing procedure. Peaks corresponding to crystalline zero valent iron, iron carbide, or hematite were not observed for Fe–C materials prepared from nitrate-based salts.

Bulk elemental analysis of Fe–C products is presented in Table 2, with oxygen content determined by difference. Carbon content increases with increasing pyrolysis temperature for both precursor systems while hydrogen and oxygen content decrease; this is consistent with pyrolysis of oxygen

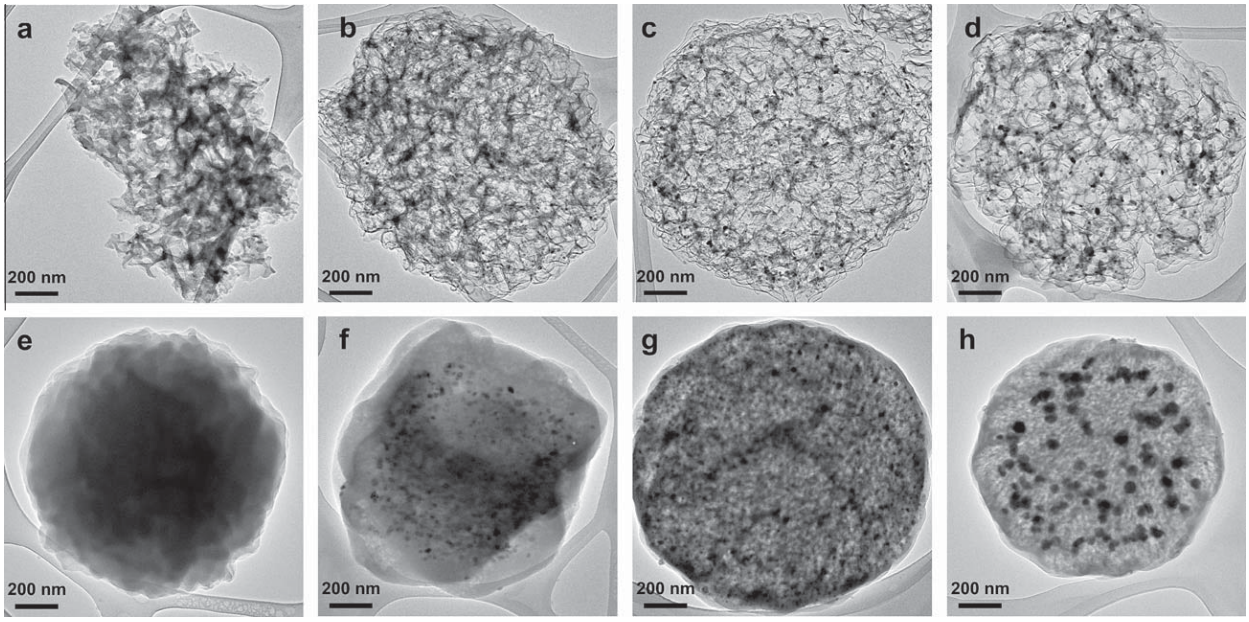

Fig. 2 – TEM images of Fe–C described in Table 1 and prepared by USP using (a–d) chloride-based precursors and (e–h) nitrate-based precursors at 500, 600, 700, and 800 °C (left to right).

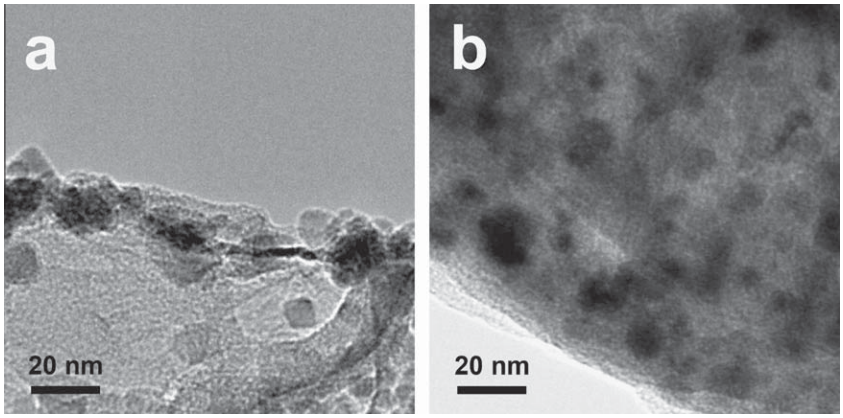

Fig. 3 – High resolution TEM images showing iron nanoparticles impregnated in the Fe–C spheres prepared using (a) chloride-based precursors at 600 °C and (b) nitrate-based precursors at 700 °C.

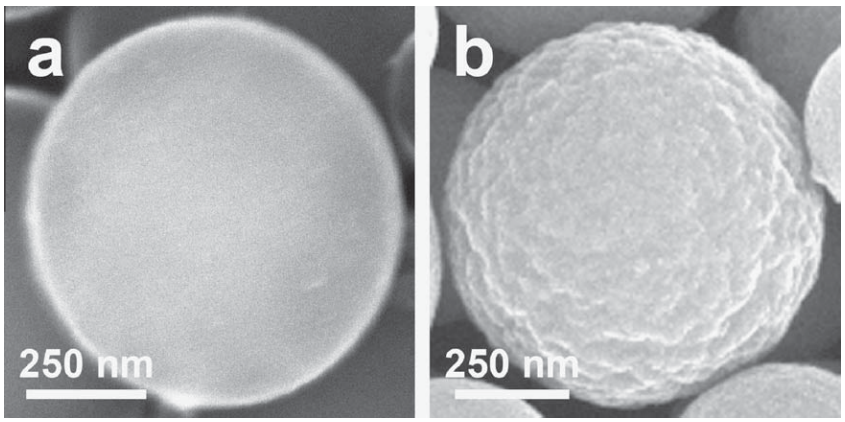

Fig. 4 – SEM images of USP Fe–C prepared from a precursor solution containing (a) 0.6 M sucrose and 0.12 M $FeCl_3$ at 900 °C, and (b) 0.5 M sucrose and 0.02 M $Fe(NO_3)_3$ at 700 °C.

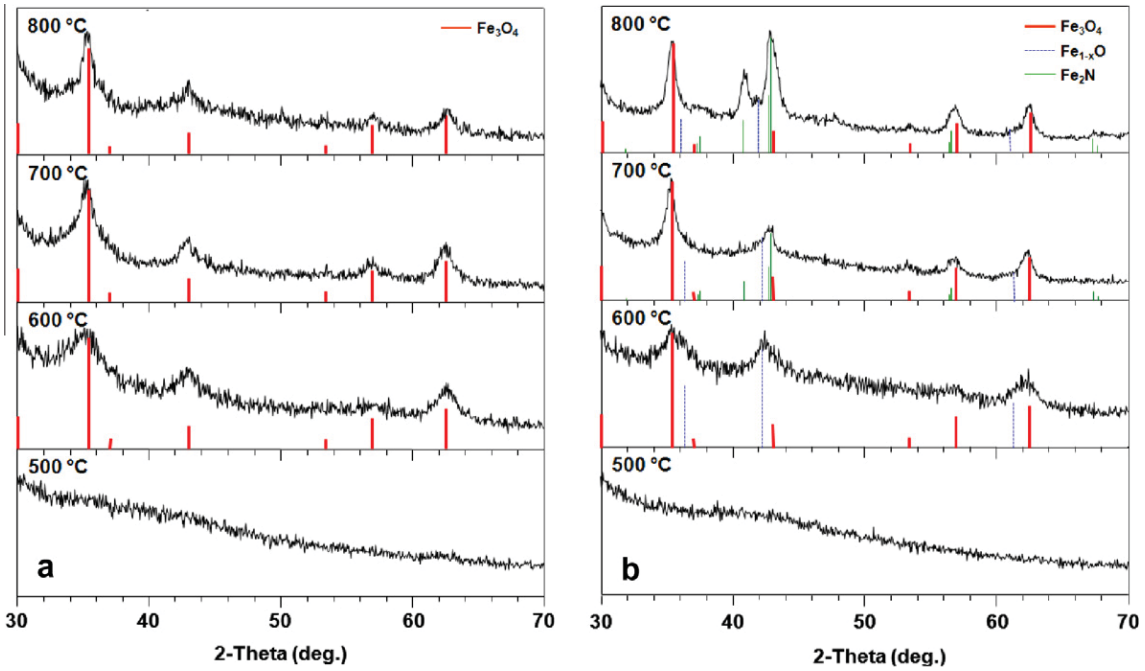

Fig. 5 – XRD patterns for Fe–C materials described in Table 1 and prepared at 500–800 °C using (a) chloride-based precursors and (b) nitrate-based precursors.

Table 2 – Bulk elemental analysis of Fe–C products, prepared at various temperatures and carrier gas flow rate of 1 SLPM, originally described in Table 1.

Figs. 1 and 2 label	Anion	Pyrolysis temp. (°C)	C (wt.%)	H (wt.%)	N (wt.%)	Fe (wt.%)	O (wt.%, by difference)
a	Chloride	500	65.1	3.3	0.3	4.0	27.3
b	Chloride	600	70.2	2.6	0.4	8.3	18.5
c	Chloride	700	73.3	2.0	0.3	9.6	14.8
d	Chloride	800	81.2	1.5	0.4	5.1	11.8
e	Nitrate	500	54.9	2.5	5.7	2.5	34.4
f	Nitrate	600	59.3	2.5	6.3	3.2	28.7
g	Nitrate	700	64.4	2.3	6.1	3.7	23.5
h	Nitrate	800	67.9	1.7	3.4	8.3	18.7

functional groups at higher temperatures, which creates a more hydrophobic material. Higher carbon concentrations and lower oxygen concentrations in the Fe–C materials prepared using the chloride-based precursors suggest increased hydrophobicity compared to those prepared from nitrate-based precursors.

Yields for collected carbon are less than 12% of the total input carbon from sucrose for all Fe–C presented in Table 1, but a separate determination between non-decomposed sucrose and gasified carbon cannot be made with the available data. The carbon yield decreases with increasing temperature, which is expected from secondary pyrolytic reactions at higher temperatures.

3.2. Precursor decomposition and Fe–C formation mechanisms

3.2.1. Formation of carbon support

Spray pyrolysis of a sucrose-only solution does not produce carbon products using the described USP system because the aerosol residence time in the furnace is insufficient to carbonize sucrose, even when high temperatures (900 °C) and decreased flow rates 8.33×10^{-6} m^3/s (0.5 SLPM) are used. The residence time under those conditions is estimated to be 7 s. Similarly, no carbon products are obtained from a sucrose/NaCl solution under our experimental conditions.

For USP with short residence times, carbon products from chloride-based precursors are only produced in the presence of a catalyst, in this case, Fe^{3+} ions acting as a Lewis acid catalyst [37]. Furthermore, iron oxide nanoparticles may act as catalytic seeds for the growth of carbon nano-structures similar to the formation of other carbon-based nanomaterials including carbon nanotubes and carbon nanocages [38–40].

Interestingly, an aqueous solution containing only sucrose and $NaNO_3$ produced solid carbon products via USP at temperatures as low as 600 °C. Unlike sodium chloride, which is chemically inert under the conditions used in this study, sodium nitrate is a strong oxidizer [41]. Decomposition products from $NaNO_3$, including O_2 and NO_2, are oxidizing agents and may catalyze sucrose dehydration or decomposition, allowing

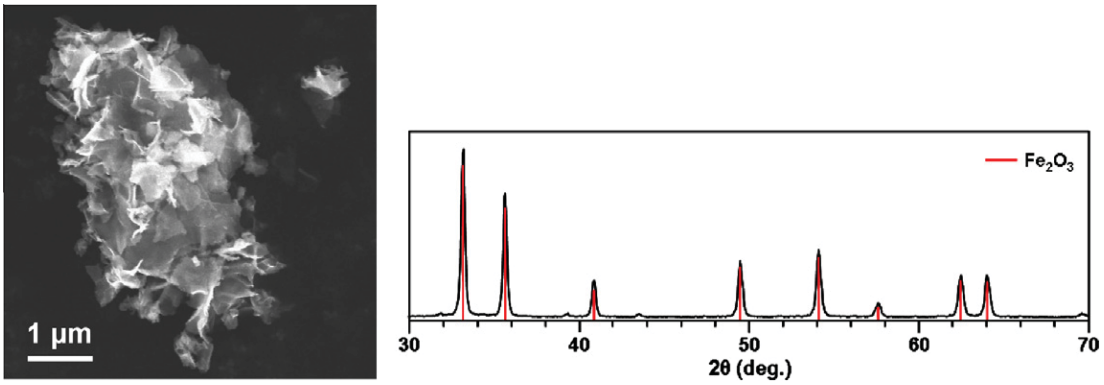

Fig. 6 – SEM image and XRD pattern of porous hematite (α-Fe_2O_3) prepared using USP at 400 °C with an aqueous solution of NaCl and $FeCl_3$ (BET surface area = 200 m^2/g).

Table 3 – Proposed paths to carbon porosity generation in Fe–C materials prepared using chloride and nitrate salts at various temperatures by the USP method.

Pyrolysis temp. (°C)	Precursor salt component	
	Nitrate precursor	Chloride precursor
500–600 700–800	• Molten $NaNO_3$, in situ template • Carbon gasification by steam from aerosol droplets or NO_2 and O_2 from nitrate salt decomposition • Molten NaOH, in situ template • Chemical activation of carbon precursor through reaction with NaOH	• Solid NaCl, in situ temple • Carbon gasification by steam from aerosol droplets • Solid NaCl, in situ template

for carbon isolation without iron [42]. Carbons prepared from an aqueous solution containing only sucrose and $NaNO_3$ at 600, 700, and 800 °C have surface areas of 20, 800, and 560 m^2/g, respectively. An aqueous precursor solution containing only sucrose and $Fe(NO_3)_3$ yields negligible product at 700 °C, preventing BET surface area analysis. In stark contrast to the chloride system, it is clear that the sodium salt in the nitrate system has more impact on carbon isolation than the iron salt.

3.2.2. *Formation of iron-based nanoparticles within carbon spheres*

Both iron nitrate and iron chloride are common catalyst precursors for incipient wetness and excess solution impregnations [43]. Evaporation of water from the USP generated aerosol droplets at the heated reactor entrance results in the formation of α-Fe_2O_3 (PDF#04-003-2900) upon heating [44]. We have observed that USP of sucrose-free chloride precursor solutions results in formation of hematite (Fig. 6).

Iron oxide reduction to magnetite or wustite must take place through reactions involving sucrose in both precursor solutions. Two possible mechanisms are proposed. First, in acidic solutions (as in aqueous $Fe(NO_3)_3$ or $FeCl_3$), sucrose is partially hydrolyzed to glucose and fructose [45,46]. As aerosol droplets enter the reactor and water evaporates, solid particles containing glucose, fructose, sucrose, NaCl or $NaNO_3$, and ferric hydroxide form. As the temperature increases, ferric hydroxide will be reduced by reaction with glucose to form reduced iron species, gluconic acid, and hydrogen [45]. Second, if Fe_2O_3 initially forms when water evaporates, it may be reduced to Fe_3O_4 or other reduced iron species by CO and H_2 (products from sucrose, glucose, and/or fructose pyrolysis and gasification). Crystalline hematite (α-Fe_2O_3) is not observed in any Fe–C products, so if it were initially formed, its conversion to crystalline, reduced iron species including Fe_3O_4 and $Fe_{1-x}O$ must occur fully. Although oxidizing gases may be generated from nitrate salt decomposition, the only crystalline species observed are reduced iron oxides, suggesting that the impact of these low concentration gases on the chemistry of the impregnated iron oxides is negligible.

In the nitrate system, it is proposed that nitriding of iron oxides occurs through reactions with NO_x at 700 and 800 °C (Table 1). Nitriding of iron in steel using potassium or sodium

Table 4 – Impact of salt presence and reactor temperature on total Fe–C surface area (S.A.) for 0.12 M $FeCl_3$ precursor solutions at a carrier gas flow rate of 0.5 SLPM.

Reactor temp. (°C)	S.A. with NaCl (m^2/g)	S.A. without NaCl (m^2/g)
600	390	10
700	520	200
900	530	710

nitrate salt baths at 650 °C is attributed to nitrides generated indirectly from nitrate decomposition, or to NO or NO_2 generated directly from nitrate decomposition [47–49].

The crystal structure of iron oxide nanoparticles depends on the reaction temperature and precursor composition. At 500 °C, crystallization of iron oxide nanoparticles does not occur rapidly, which results in formation of only amorphous iron species. While ICP-MS confirms the presence of bulk iron in materials prepared at 500 °C from both precursor solutions and TEM images show the presence of iron nanoparticles in these samples, XRD analysis does not show any evidence of crystalline iron phases (Table 2, Figs. 2 and 5). In comparison, at 600–800 °C, XRD shows the presence of crystalline iron oxide nanoparticles in the Fe–C products. Sintering of magnetite nanoparticles is minor in the chloride system but more significant in the nitrate system at increased reaction temperatures (Table 1), as evidenced by visual observation of the nanoparticles by TEM.

3.2.3. *Porosity formation in Fe–C materials*

Table 3 describes different possibilities for formation of porosity in carbon supports at various temperatures for the two precursor solutions.

For chloride-containing precursors, pore development likely occurs via two pathways, depending on temperature. At temperatures less than 700 °C, pore development results from carbon atoms networking around an *in situ* solid salt template: when water evaporates during initial droplet heating, solid NaCl (melting point = 800 °C) remains as a non-reactive inert porogen, providing a solid surface around which isolated carbon atoms can network, thus resulting in the development of an interior porous structure [19,24–26]. When this salt template is dissolved in the collection bubblers, the porous network remains throughout the carbon matrix. At 600 °C, iron-impregnated carbon materials prepared with NaCl in the precursor solution have a surface area of 390 m^2/g, whereas carbon materials prepared without NaCl are 10 m^2/g (Table 4). Despite increased water concentrations in the gas stream, carbon gasification is not expected to add surface area to Fe–C products prepared at less than 700 °C under our experimental conditions. Literature indicates that carbon gasification is significantly increased with temperature. For example, rate of CO evolution increases several times for steam gasification of coal and active carbon when the temperature increases from 700 to 800 °C [50].

It is worth noting here that hematite products prepared using USP and aqueous precursor solutions containing only NaCl and $FeCl_3$ also benefit from this *in situ* solid salt template. As-produced hematite surface areas are as high as 200 m^2/g when prepared from precursors with large (10:1) NaCl to $FeCl_3$ ratios (Fig. 6). Hematite prepared under similar pyrolysis conditions but from a precursor with a small (0.05:1) NaCl to $FeCl_3$ ratio only has a specific surface area of 30 m^2/g.

Above 700 °C, a different Fe–C pore formation mechanism is proposed for Fe–C prepared from chloride salts. At these temperatures, fresh edge-site carbon atoms formed from sucrose dehydration will react with steam in the pyrolysis gas to generate additional porosity in the carbon support. Steam gasification of carbon produces H_2 and CO, which may also be responsible for the observed reduction of iron species within the Fe–C products. In addition, steam gasification may also be catalyzed by the presence of iron nanoparticles within the carbon spheres [51,52]. With this high temperature mechanism, the presence of salt may actually hinder porosity development, since NaCl (solid or molten depending on temperature) may block carbon sites and prevent gasification. At 900 °C, materials prepared with the NaCl template have a surface area of 530 m^2/g while those materials prepared without the salt template exceed 700 m^2/g (Table 4), suggesting that the contribution of the *in situ* salt template to porosity development diminishes at higher reaction temperatures. Temperatures around 700 °C appear to be ideal for preparing Fe–C materials from chloride-based precursors in terms of surface areas and yields (Tables 1 and 4).

High and low temperature mechanisms also appear to be present for porosity development in Fe–C materials prepared using nitrate precursors. At low temperatures (500–600 °C), only low porosity materials are generated (surface areas <40 m^2/g). Carbon templating onto molten $NaNO_3$ likely contributes the minimal porosity that is observed. The absence of accessible internal porosity from surface heterogeneities, as is observed in low temperature chloride-based Fe–C products benefiting from the NaCl template, results in lower surface area materials for the nitrate precursors compared to the chloride precursors (Table 1).

As with the chloride-based precursors, carbon gasification by steam is expected to be the dominant source of porosity development in the nitrate-based Fe–C products at temperatures greater than 700 °C. Minimal porosity generation is expected from gasification by oxidizing gases (O_2, NO_2) evolved from sodium nitrate decomposition, since their concentrations are low compared to steam. The surface area of the materials prepared using nitrate salts at 700 °C is 680 m^2/g, compared to only 40 m^2/g at 600 °C (Table 1). Additional porosity may result from a molten NaOH *in situ* template that forms from the reaction of water with Na_2O, a byproduct of $NaNO_3$ decomposition. Chemical activation from reaction between NaOH and carbon may also develop porosity within the Fe–C products, though the extent of this impact is not currently clear [53]. It appears that under the test conditions employed, 700 °C is the optimum temperature to balance high yield and high surface area when using the nitrate precursors.

3.3. *Application potential of USP process and Fe–C products*

3.3.1. *Catalyst accessibility – gas and liquid phase applications*

Despite high *bulk* iron contents, quantitative analyses by XPS confirm that there are negligible amounts of iron on the outer surface of Fe–C products (both as-produced and hydrogen treated). This deficiency of external surface iron may affect the application of these Fe–C materials: for example, if the iron nanoparticles are covered by carbon, then they may not be accessible to gases and this could limit their applications as a catalyst or in other applications where gas–solid contact is required. On the other hand, liquid phase reactions, where electron transfer can occur through the carbon shell, might still be possible. Iron leaching experiments support high

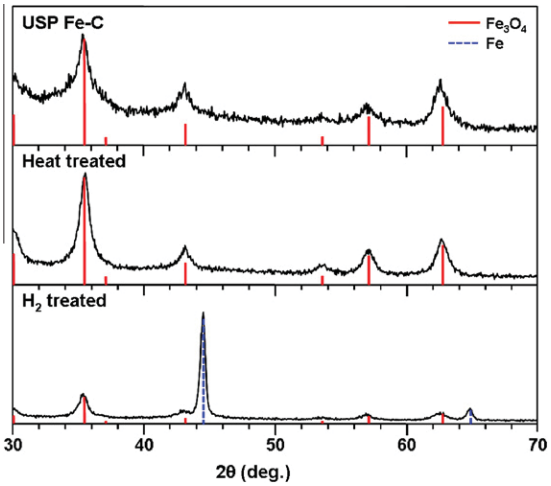

Fig. 7 – XRD patterns for Fe–C materials as prepared by USP and after heat or hydrogen treatment. The USP Fe–C sample was prepared using chloride salts at 600 °C, 0.5 SLPM N_2, 0.39 M $FeCl_3$.

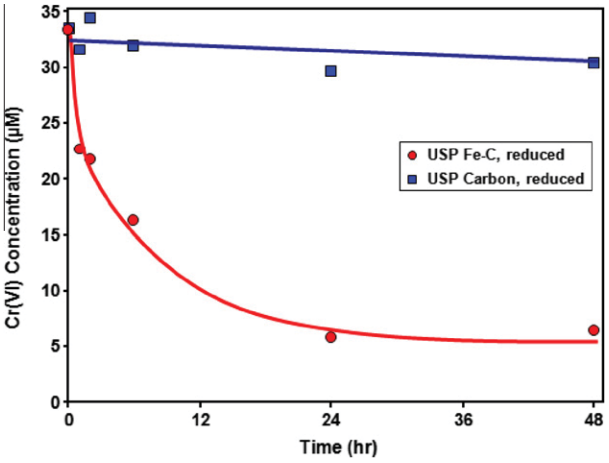

Fig. 8 – Chromium reduction using reduced Fe–C prepared from nitrate-based precursors, containing 8 wt.% Fe.

Fe–C (prepared from both nitrate and chloride salts) stability in acidic conditions, as a negligible amount of iron (<0.2%) is removed after stirring for 48 h at pH 2.

To assess iron nanoparticle accessibility, a USP Fe–C material, prepared using chloride salts, was annealed under nitrogen or hydrogen at 400 °C (to minimize the sintering of metal nanoparticles) and then analyzed with XRD to determine the structure of impregnated iron (Fig. 7). Table 5 shows the relevant physical properties of the tested materials.

Both heat alone and especially treatment with hydrogen increase the surface area of Fe–C. Heat or hydrogen treatments do not cause shifts in the Fe–C XRD pattern; zero valent iron (PDF#00-006-0696), however, is *only* present in H_2-treated Fe–C (Fig. 7). Since gas/solid contact is required for iron oxide reduction, this provides evidence that some of the impregnated magnetite nanoparticles are, at the very least, accessible to H_2 during the heat treatments. In this particular example, H_2 reduced approximately 50% of the available iron. While minor sintering of magnetite was present after the heat treatments, ZVI nanoparticles were more susceptible to sintering.

As a separate probe of catalytic activity, a reduced Fe–C sample prepared using nitrate salts was tested for reduction of aqueous hexavalent chromium to see if the iron nanoparticles were active catalytic sites for liquid-phase reduction applications. USP carbon prepared from a precursor solution containing only sucrose and $NaNO_3$ was used as a control. Both materials received the same H_2 treatment before Cr(VI) experiments.

After 48 h of exposure to the Fe–C material, Cr(VI) was reduced from 34 to 6 μM. Solutions that were treated with non-impregnated carbon contained 31 μM Cr(VI) after the same time period (Fig. 8, lines drawn to guide the eyes). It is not clear whether the improved performance of the Fe–C material is attributed to liquid–solid contact or electron transfer through the carbon shell, but the Fe–C material clearly performs well compared to pure carbon in this preliminary aqueous phase test.

3.3.2. *High iron loading Fe–C materials and their magnetic properties*

Traditional metal impregnation techniques make it difficult to attain high mass loadings onto supports while maintaining well-dispersed, metal nanoparticles. The USP process described here can produce high bulk iron loadings into porous carbon supports without sacrificing dispersion. Fig. 9 shows TEM images of Fe–C prepared from a chloride-based precursor containing 0.23 M $FeCl_3$ at 600 °C and carrier gas flow rate of 0.5 SLPM. Bulk iron analysis indicates that this material contains 35 wt.% Fe, and TEM images show that the iron oxide nanoparticles remain <20 nm. The ability to prepare such high loadings of iron nanoparticles while retaining high dispersion is exceptionally rare.

Prepared Fe–C materials containing high loadings of crystalline magnetite are magnetic. Fig. 10 shows how these materials can be isolated from water dispersions using a large magnet located to the right of the vial containing the dispersion. Presumably, a similar system could be used to remove the Fe–C powder from gas dispersions. This strong magnetism may improve the application potential of these impreg-

Table 5 – Physical properties of Fe–C before and after heat treatments under nitrogen and hydrogen.

Treatment	S.A. (m^2/g)	Fe_3O_4 (wt.%[a])	Fe (wt.%[a])	Fe_3O_4 diameter (nm)	Fe diameter (nm)
As prepared	300	100%	0%	7.5	–
Heat in N_2 (12 h, 400 °C)	490	100%	0%	9.8	–
Heat in H_2 (12 h, 400 °C)	630	57%	43%	10.2	25.0

[a] wt.% of total iron species.

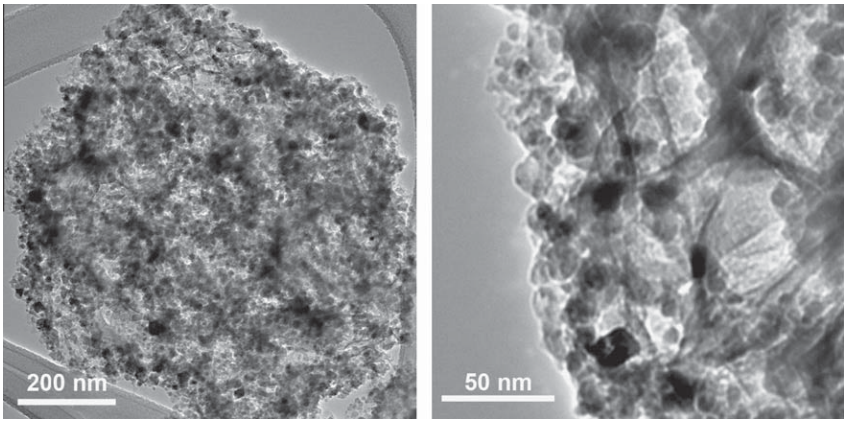

Fig. 9 – TEM images of Fe–C product containing 35% bulk iron content with average magnetite (dark black spots) diameter <20 nm.

nated carbon materials by providing a facile route to catalyst recovery.

3.3.3. USP carbon impregnation with other metals

Preliminary tests have shown that sucrose dehydration/decomposition can also be catalyzed by solutions containing Co^{2+}, Ni^{2+}, Cu^{2+}, or Zn^{2+} cations when using USP. The reaction rates for these dehydrating agents are apparently slower than with iron, which results in lower carbon production rates. The final morphology of the carbon support and metal nanoparticles, however, is similar to the Fe–C materials. Porosity development is again evidenced by increased product surface areas (Table 6).

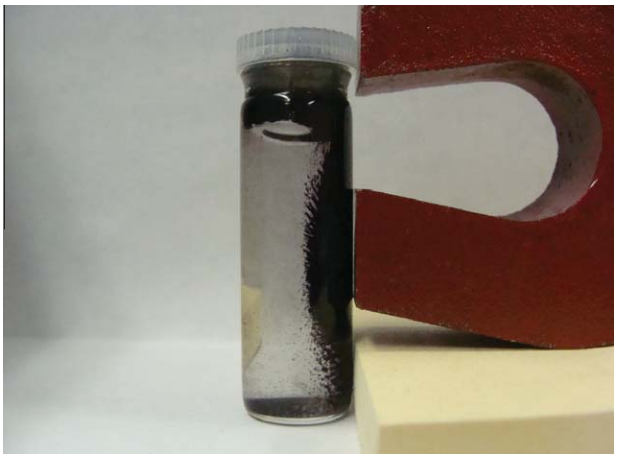

Fig. 10 – Magnetic separation of the Fe–C composite from a suspension in water.

4. Summary and conclusions

Porous carbon spheres impregnated with nanoscale magnetite, wustite, or iron nitride particles (Fe–C) can be prepared in a single-step, continuous process using ultrasonic spray pyrolysis (USP). This work simplifies established processes for preparing impregnated carbon materials, by permitting carbonization, pore formation, metal impregnation, and metal activation to occur simultaneously in a continuous process requiring little manual control. Furthermore, this process requires only a single heating step and uses low cost starting materials. Fe–C surface areas ranged from 4 to 320 m^2/g when prepared using only *in situ* templating, but exceeded 700 m^2/g from *in situ* carbon gasification or chemical activation with reaction temperatures >700 °C. Materials prepared using chloride and nitrate salts were structurally different. For chloride- and nitrate-based precursors, 700 °C was the optimal production temperature for maximizing surface area, iron dispersion, and yield. USP Fe–C materials may be useful in industrial applications due to their potential for high-loading of well-dispersed metal nanoparticles.

Table 6 – Preparation conditions and specific surface areas (S.A.) for metal-C materials prepared by USP.

Metal source	Inorganic salt	Precursor metal conc. (wt.%)	Pyrolysis temp. (°C)	Carrier gas flow rate (SLPM)	S.A. (m^2/g)
$Cu(CH_3OO)_2$ + HCl[a]	NaCl	8	600	0.5	150
$Zn(CH_3OO)_2$	NaCl	8	600	0.5	220
$Ni(NO_3)_2{\cdot}6H_2O$	$NaNO_3$	4	700	1.0	570
$Co(NO_3)_2{\cdot}6H_2O$	$NaNO_3$	4	700	1.0	480

[a] HCl added to prevent precipitation of copper hydroxide.

Acknowledgments

EPRI is acknowledged as the main funding source for this research for J.D.A., S.A.D., and M.R.A. The University of Illinois and the Air and Waste Management Association are recognized for funding for J.D.A. and M.J.R. Funding for M.E.F. and K.S.S. was provided by the US NSF DMR 0906904. SEM, TEM, XPS, and XRD were carried out in part in the Frederick Seitz Materials Research Laboratory Central Facilities, University of Illinois, which are partially supported by the US Department of Energy under Grants DE-FG02-07ER46453 and DE-FG02-07ER46471.

REFERENCES

[1] Enthaler S, Junge K, Beller M. Sustainable metal catalysis with iron: from rust to rising star. Angew Chem Int Ed Engl 2008;47(18):3317–21.
[2] Giasuddin ABM, Kanel SR, Choi H. Adsorption of humic acid onto nanoscale zerovalent iron and its effect on arsenic removal. Environ Sci Technol 2007;41(6):2022–7.
[3] Wu KT, Kuo PC, Yao YD, Tsai EH. Magnetic and optical properties of Fe_3O_4 nanoparticle ferrofluids prepared by coprecipitation technique. IEEE Trans Magn 2001;37(4I):2651–3.
[4] Shipway AN, Katz E, Willner I. Nanoparticle arrays on surfaces for electronic, optical, and sensor applications. Chemphyschem 2000;1(1):18–52.
[5] Tran N, Pareta R, Taylor E, Webster TJ. Iron oxide nanoparticles: novel drug delivery materials for treating bone diseases. Adv Mater Res 2010;89–91:411–8.
[6] Chertok B, Moffat BA, David AE, Yu F, Bergemann C, Ross BD, et al. Iron oxide nanoparticles as a drug delivery vehicle for MRI monitored magnetic targeting of brain tumors. Biomaterials 2008;29(4):487–96.
[7] Huber DL. Synthesis, properties, and applications of iron nanoparticles. Small 2005;1(5):482–501.
[8] Lide DR. In: CRC handbook of chemistry and physics. Boca Raton, FL: CRC Press; 2001.
[9] Davis BH. Fischer–Tropsch synthesis: relationship between iron catalyst composition and process variables. Catal Today 2003;84(1–2):83–98.
[10] Jaouen F, Marcotte S, Dodelet J-P, Lindbergh G. Oxygen reduction catalysts for polymer electrolyte fuel cells from the pyrolysis of iron acetate adsorbed on various carbon supports. J Phys Chem B 2003;107(6):1376–86.
[11] Bian G, Oonuki A, Kobayashi A, Koizumi N, Yamada M. Syngas adsorption on precipitated iron catalysts reduced by H_2, syngas or CO and on those used for high-pressure FT synthesis by *in situ* diffuse reflectance FTIR spectroscopy. Appl Catal A Gen 2001;219(1–2):13–24.
[12] Lin H-Y, Chen Y-W, Wang W-J. Preparation of nanosized iron oxide and its application in low temperature CO oxidation. J Nanopart Res 2005;7(2–3):249–63.
[13] Wang HC, Chang SH, Hung PC, Hwang JF, Chang M-B. Catalytic oxidation of gaseous PCDD/Fs with ozone over iron oxide catalysts. Chemosphere 2008;71(2):388–97.
[14] Rodriguez-Reinoso F. The role of carbon materials in heterogeneous catalysis. Carbon 1998;36(3):159–75.
[15] Leonhardt P, Sulimma A, van Heek K-H, Juntgen H. Steam gasification of German hard coal using alkaline catalysts: effects of carbon burn-off and ash content. Fuel 1983;62:200–4.
[16] Radovic LR, Rodriguez-Reinoso F. Carbon materials in catalysis. In: Thrower PA, editor. Chemistry and physics of carbon, vol. 25. New York: Dekker; 1975. p. 243–358.
[17] Suslick KS, Price GJ. Applications of ultrasound to materials chemistry. Annu Rev Mater Sci 1999;29:295–326.
[18] Bang JH, Suslick KS. Applications of ultrasound to the synthesis of nanostructured materials. Adv Mater 2010;22:1039–59.
[19] Skrabalak SE. Ultrasound-assisted synthesis of carbon materials. Phys Chem Chem Phys 2009;11(25):4930–42.
[20] Hampsey JE, Hu Q, Rice L, Pang J, Wu Z, Lu Y. A general approach towards hierarchical porous carbon particles. Chem Commun 2005:3606–8.
[21] Yan Y, Zhang F, Meng Y, Tu B, Zhao D. One-step synthesis of ordered mesoporous carbonaceous spheres by an aerosol-assisted self-assembly. Chem Commun 2007:2867–9.
[22] Hu Q, Lu Y, Meisner GP. Preparation of nanoporous carbon particles and their cryogenic hydrogen storage capacities. J Phys Chem C 2008;112:1516–23.
[23] Kodas TT, Hampden-Smith MJ. Aerosol processing of materials. New York: Wiley-VCH; 1999.
[24] Skrabalak SE, Suslick KS. Porous carbon powders prepared by ultrasonic spray pyrolysis. J Am Chem Soc 2006;128(39):12642–3.
[25] Skrabalak SE, Suslick KS. Carbon powders prepared by ultrasonic spray pyrolysis of substituted alkali benzoates. J Phys Chem C 2007;111:17807–11.
[26] Fortunato ME, Rostam-Abadi M, Suslick KS. Nanostructured carbons prepared by ultrasonic spray pyrolysis. Chem Mater 2010;22:1610–2.
[27] Bang JH, Han K, Skrabalak SE, Kim H, Suslick KS. Porous carbon supports prepared by ultrasonic spray pyrolysis for direct methanol fuel cell electrodes. J Phys Chem C 2007;111:10959–64.
[28] Liu H, Song C, Tang Y, Zhang J, Zhang J. High-surface-area CoTMPP/C synthesized by ultrasonic spray pyrolysis for PEM fuel cell electrocatalysts. Electrochim Acta 2007;52:4532–8.
[29] Hampden-Smith M, Antanassova P, Kodas TT. Fuel cell technology and application. In: Wielstich W, Gasteiger HA, Lamm A, editors. Handbook of fuel cells – fundamentals technology, and applications, vol. 3. John Wiley and Sons; 2003 [chapter 40].
[30] Yu G, Sun B, Pei Y, Xie S, Yan S, Qiao M, et al. Fe_xO_y@C spheres as an excellent catalyst for Fischer–Tropsch synthesis. J Am Chem Soc 2010;132:935–7.
[31] Zheng R, Meng X, Tang F. High-density magnetite nanoparticles located in carbon hollow microspheres with good dispersibility and durability: their one-pot preparation and magnetic properties. Eur J Inorg Chem 2009;20:3003–7.
[32] Yu F, Wang JN, Sheng ZM, Su LF. Synthesis of carbon-encapsulated magnetic nanoparticles by spray pyrolysis of iron carbonyl and ethanol. Letters to the editor. Carbon 2005;43:3002–39.
[33] Wang JN, Zhang L, Yu F, Sheng ZM. Synthesis of carbon encapsulated magnetic nanoparticles with giant coercivity by a spray pyrolysis approach. J Phys Chem B 2007;111:2119–24.
[34] Bystrzejewski M, Karoly Z, Szepvolgyi J, Kaszuwara W, Huczko A, Lange H. Continuous synthesis of carbon-encapsulated magnetic nanoparticles with a minimum production of amorphous carbon. Carbon 2009;47:2040–8.
[35] Wang Z, Xiao P, He N. Synthesis and characteristics of carbon encapsulated magnetic nanoparticles produced by a hydrothermal reaction. Carbon 2006;44:3277–84.
[36] United States Environmental Protection Agency (US EPA). Method 7196A, chromium, hexavalanet (colorimetric). Revised July 1992.
[37] Ermolenko IN, Lyubliner IP, Gulko NV. Chemically modified carbon fibers and their applications. Weinheim, Germany: Wiley-VCH; 1989. p. 134–6.

[38] Moisala A, Nasibulin AG, Kauppinen EI. The role of metal nanoparticles in the catalytic production of single-walled carbon nanotubes – a review. J Phys Condens Mater 2003;15:3011–35.
[39] Yoshida H, Takeda S, Uchiyama T, Kohno H, Homma Y. Atomic-scale *in situ* observation of carbon nanotube growth from solid state iron carbide nanoparticles. Nano Lett 2008;8(7):2082–6.
[40] Li H, Zhao N, He C, Shi C, Du X, Li J. Catalytic synthesis of carbon nanostructures using $Fe(OH)_3$/Al as catalyst precursors. J Alloys Compd 2009;468(1–2):64–8.
[41] Sax NI, Lewis RJ. Hawley's condensed chemical dictionary. New York: Van Nostrand Reinhold Company; 1987. p. 1066.
[42] Freeman ES. The kinetics of the thermal decomposition of sodium nitrate and of the reaction between sodium nitrite and oxygen. J Phys Chem 1956;60(11):1487–93.
[43] Regalbuto J. Catalyst preparation: science and engineering. Boca Raton, FL: CRC Press; 2007.
[44] Fischer WR, Schwertmann U. The formation of hematite from amorphous iron (III) hydroxide. Clay Clay Miner 1975;23(1):33–7.
[45] Sun X, Zheng C, Zhang F, Yang Y, Wu G, Yu A, et al. Size-controlled synthesis of magnetite (Fe_3O_4) nanoparticles coated with glucose and gluconic acid from a single Fe(III) precursor by a sucrose bifunctional hydrothermal method. J Phys Chem C 2009;113:16002–8.
[46] Pinheiro-Torres A, Oliveira FAR, Silva CLM, Fortuna SP. The influence of pH on the kinetics of acid hydrolysis of sucrose. J Food Process Eng 1994;17:191–208.
[47] Shen YZ, Oh KH, Lee DN. Nitriding of steel in potassium nitrate salt bath. Scr Mater 2005;53:1345–9.
[48] Shen YZ, Oh KH, Lee DN. Nitrogen strengthening of interstitial-free steel by nitriding in potassium nitrate salt bath. Mater Sci Eng A 2006;434:314–8.
[49] Lee M-K, Kim D-S, Kim S-C, Han S-W, Kim I, Lee DN. Effect of NaCl and $CaCl_2$ additives on $NaNO_3$ bath nitriding of steel. Mater Sci Eng A 2010;527:1048–51.
[50] Miura K, Aimi M, Naito T, Hasimoto K. Steam gasification of carbon: effect of several metals on the rate of gasification and the rates of CO and CO_2 formation. Fuel 1986;65:407–11.
[51] Rodriguez-Reinoso F, Molina-Sabio M. Activated carbons from lignocellulosic materials by chemical and/or physical activation: an overview. Carbon 1992;30(7):1111–8.
[52] Xia W, Hagan V, Kundu S, Wang Y, Somsen C, Eggeler G, et al. Controlled etching of carbon nanotubes by iron-catalyzed steam gasification. Adv Mater 2007;19:3648–52.
[53] Lillo-Ródenas MA, Cazorla-Amorós D, Linares-Solano A. Understanding chemical reactions between carbons and NaOH and KOH: an insight into the chemical activation mechanism. Carbon 2003;41:267–75.